Polymer optical fiber compound parabolic concentrator tip for enhanced coupling efficiency for fluorescence based glucose sensors

Hassan, Hafeez Ul; Nielsen, Kristian; Aasmul, Søren; Bang, Ole

Published in:
Biomedical Optics Express

Link to article, DOI:
10.1364/BOE.6.005008

Publication date:
2015

Document Version
Publisher's PDF, also known as Version of record

Biomedical Optics EXPRESS

Polymer optical fiber compound parabolic concentrator tip for enhanced coupling efficiency for fluorescence based glucose sensors

Hafeez Ul Hassan,[1,*] Kristian Nielsen,[2] Soren Aasmul,[1] and Ole Bang[2]

[1]*Medtronic R&D Diabetes Denmark A/S, Agern Allé 1, 2970 Horsholm, Denmark*
[2]*DTU Fotonik, Department of Photonics Engineering, Technical University of Denmark, 2800 Kgs. Lyngby, Denmark*
[*]*hafha@fotonik.dtu.dk*

Abstract: We demonstrate that the light excitation and capturing efficiency of fluorescence based fiber-optical sensors can be significantly increased by using a CPC (Compound Parabolic Concentrator) tip instead of the standard plane-cut tip. We use Zemax modelling to find the optimum CPC tip profile and fiber length of a polymer optical fiber diabetes sensor for continuous monitoring of glucose levels. We experimentally verify the improved performance of the CPC tipped sensor and the predicted production tolerances. Due to physical size requirements when the sensor has to be inserted into the body a non-optimal fiber length of 35 mm is chosen. For this length an average improvement in efficiency of a factor of 1.7 is experimentally demonstrated and critically compared to the predicted ideal factor of 3 in terms of parameters that should be improved through production optimization.

OCIS codes: (060.2370) Fiber optics sensors; (160.5470) Polymers; (170.1470) Blood or tissue constituent monitoring; (220.4298) Nonimaging optics.

References and links

1. S. C. Warren-Smith, S. Heng, H. Ebendorff-Heidepriem, A. D. Abell, and T. M. Monro, "Fluorescence-Based Aluminum Ion Sensing Using a Surface-Functionalized Microstructured Optical Fiber," Langmuir **27**(9), 5680–5685 (2011).
2. K.-C. Liao, T. Hogen-Esch, F. J. Richmond, L. Marcu, W. Clifton, and G. E. Loeb, "Percutaneous fiber-optic sensor for chronic glucose monitoring in vivo," Biosens. Bioelectron. **23**(10), 1458–1465 (2008).
3. J. Jensen, P. Hoiby, G. Emiliyanov, O. Bang, L. Pedersen, and A. Bjarklev, "Selective detection of antibodies in microstructured polymer optical fibers," Opt. Express **13**(15), 5883–5889 (2005).
4. G. Emiliyanov, J. B. Jensen, O. Bang, P. E. Hoiby, L. H. Pedersen, E. M. Kjaer, and L. Lindvold, "Localized biosensing with Topas microstructured polymer optical fiber," Opt. Lett. **32**(5), 460–462 (2007).
5. G. Emiliyanov, P. E. Høiby, L. H. Pedersen, and O. Bang, "Selective serial multi-antibody biosensing with TOPAS microstructured polymer optical fibers," Sensors (Basel) **13**(3), 3242–3251 (2013).
6. N. Polley, S. Singh, A. Giri, P. K. Mondal, P. Lemmens, and S. K. Pal, "Ultrafast FRET at fiber tips: Potential applications in sensitive remote sensing of molecular interaction," Sens. Actuators B Chem. **210**, 381–388 (2015).
7. S. Ko and S. A. Grant, "A novel FRET-based optical fiber biosensor for rapid detection of Salmonella typhimurium," Biosens. Bioelectron. **21**(7), 1283–1290 (2006).
8. K. E. Sapsford, L. Berti, and I. L. Medintz, "Materials for fluorescence resonance energy transfer analysis: Beyond traditional donor-acceptor combinations," Angew. Chem. Int. Ed. Engl. **45**(28), 4562–4589 (2006).
9. G. Chen, F. Song, X. Xiong, and X. Peng, "Fluorescent Nanosensors Based on Fluorescence Resonance Energy Transfer (FRET)," Ind. Eng. Chem. Res. **52**(33), 11228–11245 (2013).
10. R. Ballerstadt, C. Evans, A. Gowda, and R. McNichols, "Fiber-coupled fluorescence affinity sensor for 3-day in vivo glucose sensing," J. Diabetes Sci. Technol. **1**(3), 384–393 (2007).
11. A. Woehler, J. Wlodarczyk, and E. Neher, "Signal/noise analysis of FRET-based sensors," Biophys. J. **99**(7), 2344–2354 (2010).
12. S. Liu, L. Huang, C. Wang, Q. Li, and H. Xu, "Simultaneous excitation and emission enhancement of fluorescence assisted by double plasmon modes of gold nanorods simultaneous excitation and emission enhancement of fluorescence assisted by double plasmon modes of gold nanorods," J. Phys. Chem. C **117**(20), 10636–10642 (2013).

#250279 Received 17 Sep 2015; revised 16 Nov 2015; accepted 18 Nov 2015; published 20 Nov 2015

13. R. Bardhan, N. K. Grady, J. R. Cole, A. Joshi, and N. J. Halas, "Fluorescence Enhancement by Au Nanostructures: Nanoshells and Nanorods," ACS Nano **3**(3), 744–752 (2009).
14. J. K. Nielsen, J. S. Christiansen, J. S. Kristensen, H. O. Toft, L. L. Hansen, S. Aasmul, and K. Gregorius, "Clinical evaluation of a transcutaneous interrogated fluorescence lifetime-based microsensor for continuous glucose reading," J. Diabetes Sci. Technol. **3**(1), 98–109 (2009).
15. K. Tanaka, M. T. Pacheco, J. F. Brennan III, I. Itzkan, A. J. Berger, R. R. Dasari, and M. S. Feld, "Compound parabolic concentrator probe for efficient light collection in spectroscopy of biological tissue," Appl. Opt. **35**(4), 758–763 (1996).
16. W. T. Welford and R. Winston, *The Optics of Nonimaging Concentrators* (Academic New York, 1978).
17. L. C. Chen, A. L. Y. Low, and S. F. Chien, "Compound parabolic tapered fiber for fiber coupling with a highly divergent source," Appl. Opt. **43**(32), 5923–5925 (2004).
18. S. Gangadhara, "How to Model Fluorescence Using Bulk Scattering," (2008). *https://www.zemax.com/support/knowledgebase/how-to-model-fluorescence-using-bulk-scattering.*
19. G. Jiang, R. F. Shi, and A. F. Garito, "Mode coupling and equilibrium mode distribution conditions in plastic optical fibers," IEEE Photonics Technol. Lett. **9**(8), 1128–1130 (1997).
20. "Modal Effects on Multimode Fiber Loss Measurements.", *http://www.thefoa.org/tech/ref/testing/test/MPD.html.*
21. "Acrlylic Sheet Fabrication Manual.", *http://www.plexiglas.com/export/sites/plexiglas/.content/medias/downloads/sheet-docs/plexiglas-fabrication-manual.pdf*
22. W. Yuan, A. Stefani, M. Bache, T. Jacobsen, B. Rose, N. Herholdt-Rasmussen, F. K. Nielsen, S. Andresen, O. B. Sørensen, K. S. Hansen, and O. Bang, "Improved thermal and strain performance of annealed polymer optical fiber Bragg gratings," Opt. Commun. **284**(1), 176–182 (2011).
23. K. E. Carroll, C. Zhang, D. J. Webb, K. Kalli, A. Argyros, and M. C. Large, "Thermal response of Bragg gratings in PMMA microstructured optical fibers," Opt. Express **15**(14), 8844–8850 (2007).
24. A. Stefani, K. Nielsen, H. K. Rasmussen, and O. Bang, "Cleaving of TOPAS and PMMA microstructured polymer optical fibers: Core-shift and statistical quality optimization," Opt. Commun. **285**(7), 1825–1833 (2012).

1. Introduction

Fluorescence based fiber-optical sensors have been used widely to measure various physical and biological quantities of interest, such as aluminum ions [1], glucose [2], α-streptavidin and α-CRP antibodies [3–5]. A special type of these sensors uses the so-called FRET (Förster Resonance energy transfer) as the sensing mechanism [6, 7].

FRET is a phenomenon in which a radiation less energy transfer occurs between an excited donor fluorophore and a proximal ground state acceptor (a fluorophore or a dye) through a long range dipole-dipole interaction [8]. FRET can be used to measure intermolecular distances in the range of Ångstrøms (10-100Å) [9].

In a simple configuration, a FRET based sensor consists of a donor flourophore labelled on a receptor molecule specific to a particular analyte, and a molecule (ligand) labelled with a dye, which competes with the analyte in binding to the receptor. When the analyte enters the system, it competes with the ligand in binding to the receptor, thus reducing the probability of FRET, resulting in higher fluorescence and lifetime of the excited state for the donor. The change in the donor fluorescence intensity or lifetime can be used to find the concentration of the target molecule in a system.

FRET based polymer optical fiber (POF) sensors have been used for continuous in-vivo glucose sensing before [2, 10]. For these glucose sensors, plane cut fiber tips have been used. In [10] it has been suggested to reduce the input power, in order to minimize the sensor drift for accurate and continuous glucose measurements. However, one limitation of the FRET based sensors is typically the low intensity of the detected fluorescence, which leads to a low signal-to-noise ratio [11]. Reducing the excitation intensity will in this case therefore just further decrease the fluorescence intensity.

Several techniques can be used in general to improve the signal to noise ratio for FRET [11–13]. A simple solution, however, for a fiber based FRET sensor, can be to taper the fiber tip to increase its numerical aperture and thereby allow one to increase the excitation and the fluorescence light pickup efficiency. For a sensor, which is to be inserted transdermally into the human body, the sensor head should be as short as possible. This constrains the tapering lengths to a few hundred micrometers. In case of multimode fibers, such sharp linear tapering

#250279 Received 17 Sep 2015; revised 16 Nov 2015; accepted 18 Nov 2015; published 20 Nov 2015

can increase the numerical aperture, but some of the excitation and coupled fluorescence will leak out.

Therefore we here propose to use a CPC (Compound Parabolic Concentrator) polymer fiber tip for FRET based glucose sensors in order to increase the florescent signal and improve the signal to noise ratio. The CPC tip can concentrate the excitation light as well as increase the numerical aperture, even when being only a few hundred micrometers long. For portable sensors measuring continuously, the increased light capturing efficiency of the CPC fiber tip can also reduce power consumption.

The paper is divided into five sections: The first section will describe the glucose sensor configuration and its principle. The second and the third sections explain the CPC, its geometry and how it increases the numerical aperture, followed by a description of a simple Zemax model to evaluate and find the optimum geometrical parameters of a CPC for a maximum increase in excitation and fluorescence pick up efficiency. The fourth part details the manufacturing and characterization of the CPC tips. The final part compares and discusses the characterization of real CPC shapes with Zemax results.

2. The glucose sensor

Here we consider an intensity-based continuous glucose sensor based on the FRET principle. Earlier versions of this sensor employed FRET lifetime measurements for glucose sensing and were not fiber based [14]. The current version of the sensor consists of a permeable membrane bonded to a POF. The compartment formed by the membrane and fiber is filled with fluorescence assay chemistry as shown in Fig. 1.

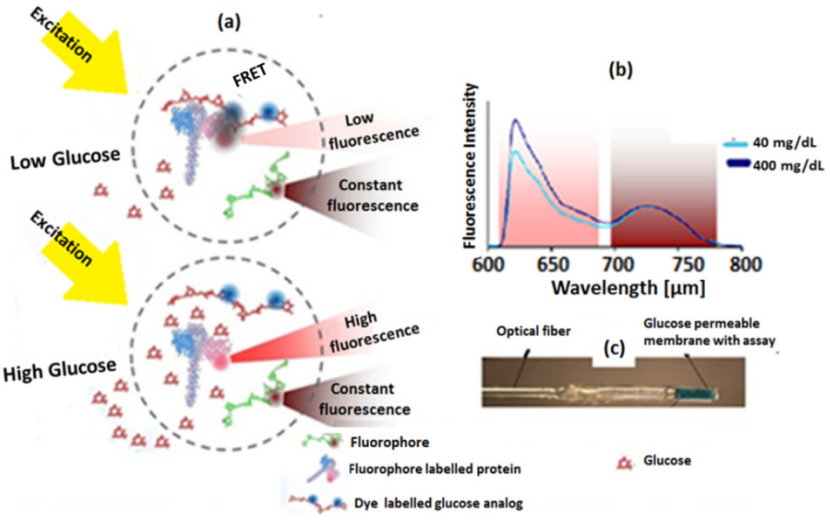

Fig. 1. MEDTRONIC Glucose Sensor and its basic sensing principle (a) Assay chemistry with FRET for low and high glucose concentration conditions resulting in (b) corresponding low and high fluorescence related to glucose levels. (c) Optical fiber bonded to assay containing membrane.

The permeable membrane allows the diffusion of glucose into the chemistry when placed in a glucose solution. The POF guides the 590 nm light for assay excitation and couples the emitted 630 nm fluorescence back to the optical interrogation unit for glucose measurement.

The assay chemistry inside the membrane consists of a glucose binding protein and a glucose analog labelled with a fluorophore and a dye, respectively, which make a FRET pair. In the presence of glucose, the glucose analog competes with the glucose on binding to the protein. The system reaches an equilibrium, which correlates with the glucose concentration. Low glucose concentration results in close proximity of the glucose binding protein and the

#250279 Received 17 Sep 2015; revised 16 Nov 2015; accepted 18 Nov 2015; published 20 Nov 2015

glucose analog. This leads to FRET between the fluorophore and the dye, resulting in decreased fluorescence intensity. High glucose concentration results in a high degree of separation of donor-acceptor pairs, leading to high fluorescence intensity. The fluorescence intensity thus correlates with the glucose concentration, as shown in the lower right part of Fig. 1.

Importantly, in the real sensor a reference fluorophore emitting at a different wavelength of 723 nm, unaffected by the glucose concentration, is included in the assay as a reference to eliminate the variations in the intensity of the light source and the optical coupling between the assay and the optical system, as illustrated in Fig. 1(a).

3. Compound parabolic concentrator

The CPC is widely used in solar energy systems, where it is required to concentrate sunlight over a large area (typically square meters) into a small collection area [15]. In two-dimensional geometry, the CPC is essentially two identical and oppositely aligned parabolas truncated at their focal point, as shown in Fig. 2(a). A detailed geometrical description of the CPC in both 2 and 3 dimensions is given in [16]. A CPC shape follows the edge ray principle illustrated in Fig. 2(b). The principle requires that if the edge rays at the input aperture i.e. rays at edge points A and A‘, reaches the edge points B and B’ at the output aperture, then all the rays incident at the input aperture within a limited acceptance angle of the CPC governed by the edge rays, will also be reflected at the boundaries to finally exit the output aperture. Any ray outside the acceptance angle will be rejected before reaching the output aperture.

The Etendue is conserved by edge ray principle [16], i.e.

$$a_1 NA_1 = a_2 NA_2 \Rightarrow a_1(n_1 \sin\theta_1) = a_2(n_2 \sin\theta_2) \tag{1}$$

where NA_1 and NA_2 are the numerical apertures at the input and output ends, respectively. This equation shows that the numerical aperture at the output is increased for the CPC tip due to its reduced output aperture diameter.

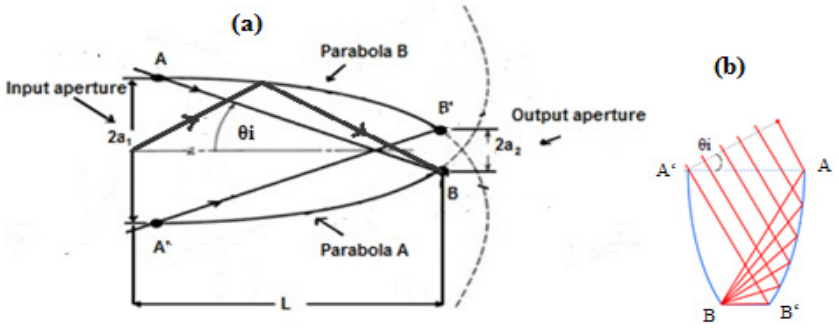

Fig. 2. (a) Geometry of a compound parabolic concentrator (CPC), (b) Edge ray principle for the CPC.

The geometrical parameters of the CPC can be derived from this principle and are given as:

$$a_1 = a_2 / \sin\theta_i \tag{2}$$

$$L = (a_1 + a_2) / \tan\theta_i \tag{3}$$

where a_1 and a_2 are radii of the input and output aperture (core diameter for the POF considered below), while θ_i and L are the acceptance angle and length of the CPC, respectively.

#250279 Received 17 Sep 2015; revised 16 Nov 2015; accepted 18 Nov 2015; published 20 Nov 2015

For a CPC viewed in the reverse direction, the edge ray principle also holds true. This means that all the rays incident upon the output aperture within its aperture angle (i.e., NA_2) will come out from the input aperture with cone angle ≤ 2 θ_i [17].

4. Zemax model

A simple Zemax model has been used to evaluate the CPC fiber tip shown in Fig. 3. A 26 degree cosine source is coupled to a multimode step-index POF (super ESKA) with a numerical aperture of NA_{POF} = 0.5 and an outer diameter of d = 250µm. The core is made of polyvinyl methacrylate (PMMA) and has a refractive index of n_{core} = 1.49 and a diameter of d_{core} = 240µm. The cladding is a 5µm thick PVDF (polyvinylidene difluoride) layer with refractive index n_{clad} = 1.40. The fiber excites an assay with a known refractive index n_{assay} = 1.33 and a known absorption and emission coefficients. The assay chemistry is enclosed in a membrane with refractive index $n_{membrane}$ = 1.45 and a thickness of 40µm.

In a real CPC fiber tip, it is the core-cladding interface, which has the actual theoretical CPC shape detailed in Section 2 (see Fig. 2(a)). The real cladding thickness and thus the outer fiber diameter simply follows the CPC-shaped core. To calculate the CPC form of the core we use the geometry seen in the inset of Fig. 3. The input aperture of the CPC is therefore the fiber core diameter $2a_1$ = 240 µm.

The CPC shaped core will transmit all the light from the straight fiber part to its output aperture and provide perfect coupling of fluorescence back to the straight part of the POF only if the acceptance angle of the CPC and the straight part of the POF matches, i.e., if $\theta_i \le (90-\theta_c) \le \cos^{-1}(n_{clad}/n_{core})$, where θ_c is the critical angle for total internal reflection at the core-cladding interface [17]. Substituting in Eq. (2), with input aperture 240µm, the matching occurs when the CPC output aperture is $2a_2$ = 82µm.

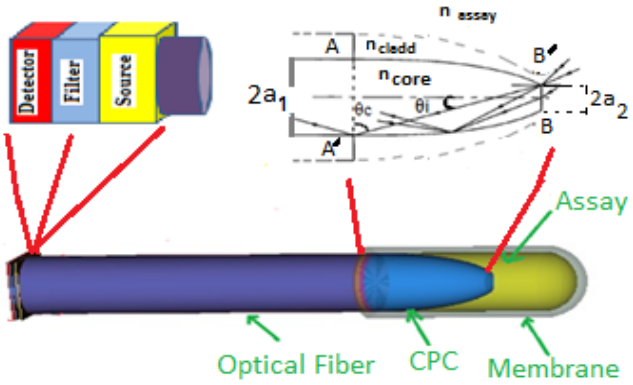

Fig. 3. Zemax model with transmission fiber and CPC tip. The left inset shows the source, filter and detector. The right inset shows the CPC configuration and geometry.

A bulk scattering model confined to one scatter event per ray is used to model the fluorescence event in the assay chemistry: Light at a first wavelength (590nm) propagates and bulk scatters isotropically in the assay and shifts to a second wavelength (630nm). The mean free path before a scatter event is set to 0.9 mm by the chemistry properties. At the input facet of the fiber a rectangular detector with the size of the fiber is placed behind an ideal optical filter that blocks the 590 nm excitation wavelength and transmits the 630 nm fluorescence signal that is picked up and guided back through the fiber. As the filter is placed behind the source and filter in the model, there is an air gap of 13µm between the fiber and the detector. Given that the loss of the Super Eska fiber is only 0.003 dB/cm at 650 nm and we consider fiber lengths shorter than 5.5cm, we neglect fiber loss in the Zemax modelling. Further details on the modelling of fluorescent sources in Zemax are given in [18].

#250279 Received 17 Sep 2015; revised 16 Nov 2015; accepted 18 Nov 2015; published 20 Nov 2015

The Zemax model has been used to find the optimum CPC shape, which gives the maximum improvement in the detected power compared to the standard plane-cut fiber for a fixed total fiber length of 5 mm (see Fig. 4). The maximum efficiency should be for an output diameter of around 82 µm, for which the CPC angle θ_i is matched to the acceptance angle of the straight part of the POF.

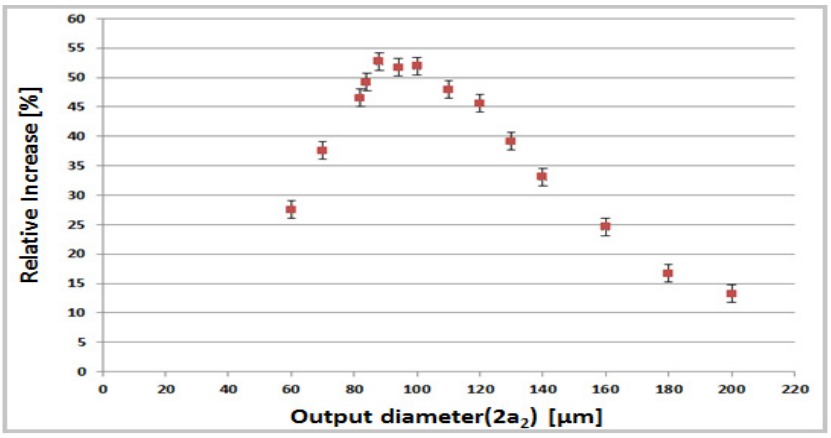

Fig. 4. Relative increase $\Delta P = |P_{CPC}-P_{plane}|/P_{plane}$ in detected fluorescence power P_{CPC} for a 5 mm long POF with a CPC tip of varying output diameter $2a_2$, as compared to the detected power of a 5 mm long straight plane-cut POF.

The maximum increase of 52% is found for a CPC with a $2a_2$ = 88 µm output aperture (core diameter) for this fiber length of 5mm close to the expected 82µm output diameter. Importantly, the increase is above 45% for an output aperture of 100 ± 20 µm, which means that the optimum CPC shape is quite tolerant to fabrication variations.

For the found optimum CPC configuration we checked that the approximation of considering only one scatter event in the model did not influence the result by repeating the calculation using multiple scattering events per ray. This gave an improvement of 51.3%, which indicates that the single scattering assumption is valid for this setting. Furthermore, in Fig. 4 each point is found as an average over 16 simulations (combinations of 4 plane-cut and 4 CPC) and the error bars indicate the standard deviation from the average value. This uncertainty comes from the limited pixel size detector used in Zemax and the finite number of rays used in the modelling. We used here 1 million rays and 50x50 pixels for the 250x250 µm rectangular detector.

As the CPCs will be used in human bodies for glucose sensing, the mechanical strength of the sensor is compromised if the output diameter of the CPC is too small. Thus for the mechanical stability, standardization, and ease of fabrication and control, we will in the following consider a CPC with the output aperture diameter of $2a_2$ = 120 µm, which has a predicted improvement of 46% and is half the original core diameter. This also fixes the length of the CPC to 311 µm.

In any optical fiber, the equilibrium modal distribution will first be reached after a certain length, which will depend on the launch conditions [19]. The equilibrium modal distribution (EMD) describes the modal distribution in a long fiber, which has lost the most lossy higher-order and leaky modes, leading to a condition where the power distribution between the remaining modes is approximately constant. In contrast, a short fiber may still hold all the power initially launched into all higher order and leaky modes. The initial rapid change in modal distribution and loss of power can be described as a transient loss [20]. Given these effects, we need to consider a range of fiber lengths in order to optimize the sensor.

We now compare the performance of a standard plane-cut sensor and a CPC tipped sensor with the optimum CPC shape (output aperture 120µm), for an identical fiber length in the

#250279 Received 17 Sep 2015; revised 16 Nov 2015; accepted 18 Nov 2015; published 20 Nov 2015

range of 311µm (CPC length) to 55 mm. As one can see from Fig. 5(a), the detected fluorescence decreases with increased fiber length for both the plane-cut and CPC tipped fiber sensor, but with different attenuation rates as expected. This is because of the different launch conditions in the two cases.

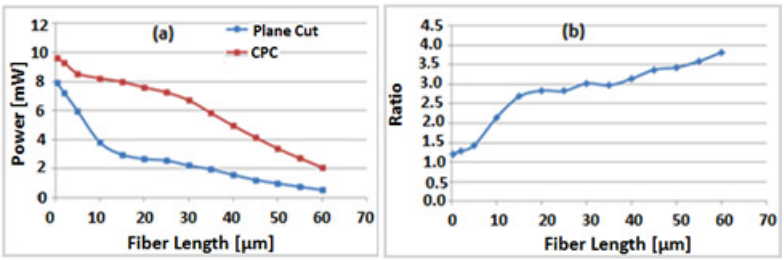

Fig. 5. Results of Zemax modelling. (a) Detected fluorescent power for a 1W 26° cosine excitation source, as a function of fiber length; (b) Ratio between fluorescent power collected by the CPC tipped and the plane cut fiber versus fiber length.

Figure 5 shows several interesting features. For a fiber of only the CPC length (i,e 311µm), the initial power for CPC tip is higher than that of a plane-cut fiber tip. This shows that the CPC efficiently excites the fluorescence chemistry resulting in more excited flourophores close to the CPC tip compared to the plane-cut fiber tip. The light from isotropically emitting flourophores will enter both fibers at all angles. As the CPC conserves etendue according to Eq. (1), the NA of the CPC tip is twice the NA of the plance-cut tip (NA_{CPC} = 1.02), which means that the coupling of fluorescence the straight fiber, will be much better for the CPC tip. In particular, all rays from the isotropically emitting flourophores that fall inside the acceptance angle will be captured and guided. For the CPC tip the acceptance angle in assay would have been close to 90° (as NA = 1.46 in Eq. (1) is much greater than unity) if the output core diameter had been 82 µm, but for this non-ideal 120 µm output core diameter it is 50°. This is still significantly greater than the acceptance angle of 22.54° of plane-cut fiber tip, which again explains the improved performance of the CPC tipped sensor.

The fluorescence power at angles outside the acceptance angle will be in the leaky modes, which will also propagate for a certain length in the fiber and may reach the detector if the fiber is short enough. The power carried in the leaky modes is different for each case and so is the model distribution. There will be more power in the leaky modes in the fiber with the plane-cut tip and thus the overall power carried by this fiber will decay more quickly compared to the CPC tipped fiber. This is seen as the rapid drop in detected power for the plane-cut fiber in Fig. 5(a).To confirm this, we plot in Fig. 6 the angular distribution of the detected fluorescence signal in radiance per solid angle.

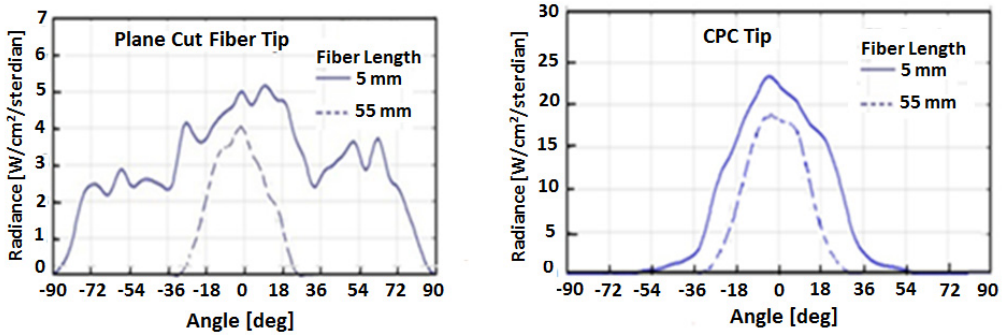

Fig. 6. Fluorescence radiance in angular space at a detector placed at the end of the fiber for fiber lengths 5 and 55 mm. (a) for plane-cut fiber tip. (b) for CPC tipped fiber.

#250279 Received 17 Sep 2015; revised 16 Nov 2015; accepted 18 Nov 2015; published 20 Nov 2015

As mentioned earlier in the model, there is a distance between the fiber and the detector. So the detector is measuring the angular distribution of the fluorescence emitted from the fiber through an air interface. Therefore for analyzing Fig. 6, we have to consider, fiber with an acceptance angle in air, which is 30°. Figure 6 shows that for the plane cut fiber tip, a significant part of the power inside the fiber is propagating at angles larger than the acceptance angle of the fiber (i.e. 30°), which corresponds to leaky modes. For the CPC tip, the power carried by the leaky modes is low. Eventually for longer lengths, such as 55 mm, both sensors loose the leaky modes and the power is carried only by the guided modes.

It is interesting to note from Fig. 5 that the optimum fiber length for the plane-cut and CPC based fiber sensor should be as short as possible. However, as the real sensor is to be inserted into the body, it needs to have a certain length. In addition a reader unit has to be attached to the sensor fiber, which further adds to the fiber length. Therefore the shortest practical fiber length is around 35 mm.

5. CPC manufacturing

The super ESKA, 0.25 mm POF with the same specifications as given in the Zemax model has been used to manufacture CPC tips with a close to ideal CPC shape. To remove residual stress from the drawing the fibers were first annealed as recommended by Akrema S/A [21] in an oven where the temperature is ramped up from 25 to 90°C at 10°C/hour and kept at this temperature for 5 min before ramping down to 25°C at 15°C/hour. Annealing is well-known to be essential for stable POF sensor operation [22, 23].

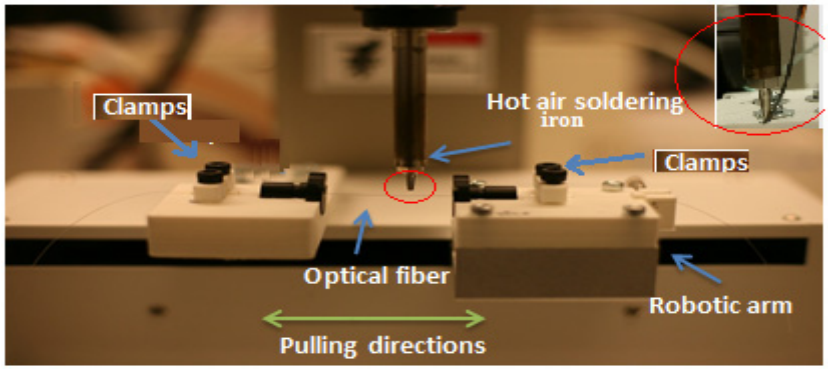

Fig. 7. Setup for CPC formation, with heat reflector shown at upper right corner.

The CPC tips were then made using a heat and pull tapering method. The setup is shown in Fig. 7. In this method an optical fiber is mounted by the clamps between the two robotic arms. A hot air soldering iron with a nozzle diameter of 2mm equipped with a stainless steel heat reflector for homogeneous heating of the fiber is used to heat the taper zone up to 190°C for 5-10 seconds. After a pre-set heating time the fiber is pulled by the robotic arms with a pre-set constant speed and pulling distance. Different parameters, such as temperature, air pressure, pulling speed, and pulling distance, were optimized to get the desired CPC shape and tapering length with specific tapering ratios suitable to make CPC tips.

An example of a tapered fiber is shown in Fig. 8. It is cut at the two places indicated in Fig. 8 and polished to the required output diameter of 125 µm .Thus each pull produces two CPCs. The dimensions of the CPCs were measured at 5X scale with a microscope, which has an uncertainty of ± 5µm.

#250279 Received 17 Sep 2015; revised 16 Nov 2015; accepted 18 Nov 2015; published 20 Nov 2015

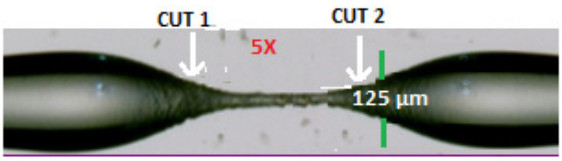

Fig. 8. Tapered optical fiber, each pull producing two CPCs which are cut at certain lengths as shown by white arrows and further on polished to required CPC output diameters.

It is well known that the hot cleaving of the polymer fiber provide better quality facet especially for the microstructure fibers [24]. However, as the fiber in our case is a step index fiber, simple cutting and polishing is sufficient to get the good quality of fiber tip facet.

The CPC tips made by this method were not completely uniform in shape. A general feature is for example that at the start of a CPC, the diameter increases. The possible reasons for not obtaining completely uniform shapes will be explained later in this section. After the process optimization, two batches each containing ten CPCs were made. Some CPCs are shown in Fig. 9. The batches were made with a time gap of 3 days between them. Furthermore, the time between each tapering process to make CPCs was approximately 10 minutes. The manufacturing parameters for the two batches are the same, except for the heating time, which was 10 and 5 seconds for the 1st and 2nd batch, respectively. The CPC batches were then tested for their optical performance.

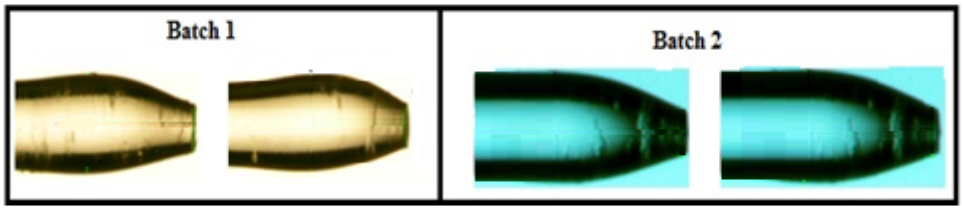

Fig. 9. Shape of CPCs from two batches: The Pulling distance was 0.8 mm, the Pulling speed was 0.4 mm/sec, and the heating time was 10 and 5 sec for Batch 1 and 2, respectively.

5.1 CPC characterization

The CPCs were characterized geometrically and optically. Two parameters were selected for the geometrical characterization:

1. Maximum diameter of the fiber at the start of the CPC.

2. Length of the CPC tip measured from the maximum diameter to the output aperture

Both parameters are shown in Fig. 10.

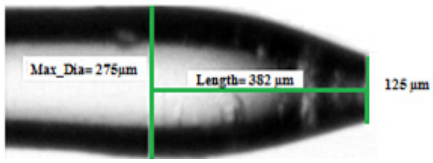

Fig. 10. CPC with its geometrical parameters for characterization.

The optical coupling efficiency was characterized using a miniature cuvette made of a non-fluorescing transparent 250um inner diameter Tygon tube sealed in one end and filled with the chemistry used in glucose sensors. The 35mm long CPC tipped fibers were inserted into the tube to form a dummy sensor and then characterized using an epi-fluorescence set-up with a fiber optical spectrometer (USB2000 + , Ocean Optics, FL, USA).

A schematic of the test setup and dummy sensor is shown in Fig. 11. In this setup, light from a broad band source (LED) HLMP-EL30-MQ000 with dominant wavelength of 590 nm

#250279 Received 17 Sep 2015; revised 16 Nov 2015; accepted 18 Nov 2015; published 20 Nov 2015

passes through a 55nm excitation filter with 560nm central wavelength and a beam splitter and is coupled to the fiber by a lens to excite the assay chemistry. The chemistry contains two types of fluorophores: The assay fluorophores have an excitation wavelength at 590 nm and an emission maximum around 630 nm and the reference fluorophore has an excitation wavelength close to 590 nm with an emission maximum at 710 nm. The resulting 630 nm and 710 nm fluorescence from the assay chemistry, is picked up by the fiber and passed through a beam splitter and a long-pass emission filter with 610 nm cut-off wavelength to finally reach the spectrometer. Fluorescence spectra from plane cut and CPC tip fibers were then compared.

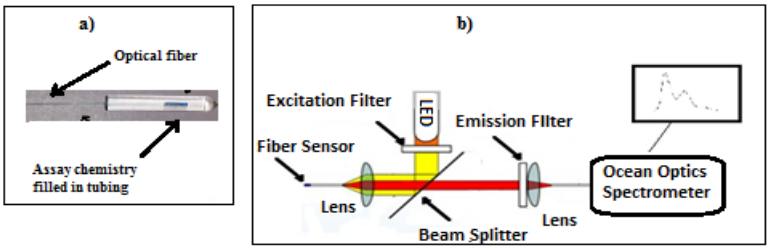

Fig. 11. (a) Dummy sensor (b) Setup for optical characterization of the CPC based sensor.

All sensors from Batch 1 and Batch 2 were tested three times. Each time the fiber is removed from the setup and the cuvette and cleaned, a new cuvette is filled with the same chemistry and the cleaned fiber is inserted into the new cuvette, and finally aligned with the characterization setup. The three repetitions allow getting a statistical average and thereby reducing the effect of any misalignment and coupling variations.

5. Results and discussion

Geometrical characterization of two batches is summarized in Table 1.

Table 1. Geometrical characterization of two batches

Max. diameter [µm] [a]Error (± 5 µm)	**Batch 1 *N = 10**	**Batch 2 N = 10**	**Length [µm] Error (± 10 µm)**	Batch 1 N = 10	Batch 2 N = 10
Batch Average	283	270	**Average**	421	429
Standard Deviation	3	7	**Standard Deviation**	27	32
Confidence Interval (95%)	[281;285]	[265;275]	**Confidence Interval (95%)**	[405;437]	[408;450]

[a]N = Sample size *Error due to Microscope inaccuracy of ± 5 µm

Both batches of CPCs manufactured by this method were not perfectly parabolic and also had some variations in their shape. In general there was a localized maximum in the diameter and the average CPC length was almost 100 µm longer than the ideal CPC length with a 125 µm output aperture (i.e., 311 µm).

This may be caused by the following reasons: 1) Increase in fiber diameter can possibly be caused by the hot air cone exerting the molten PMMA (heated well above its glass transition temperature of about 110°C) in the heating zone and pushes it towards the sides. It is also interesting to note from Table 1, that for batch 2 of CPC, the increase in the fiber diameter is reduced by optimizing the heating time to 5 sec. This explains that the possible cause for increase in the diameter is redistribution of molten PMMA. Lesser the heating time, lower is the redistribution. 2) Asymmetry in shapes can be explained by the inhomogeneous heating of the fiber. The fiber experienced more heat at the nozzle side than the reflector side. This is also because fiber is heated in an ambient environment with no control of the ambient temperature; 3) Variations in the CPC length can be because variations in manual cutting and polishing the fiber to the right output diameter.

#250279 Received 17 Sep 2015; revised 16 Nov 2015; accepted 18 Nov 2015; published 20 Nov 2015

We evaluate that the first two reasons are the most important and are working on a detailed characterization of the influence of the temperature, heating time and heat zone structure on the CPC quality. However, for the proof-of-principle of the CPC improvements presented here, our batches 1-2 are adequately demonstrating the enhancement of the fluorescence pickup efficiency.

While the CPCs fabricated by this method have a non-ideal shape, the shape they do have is maintained for all CPC with a low standard deviation maximum diameter and length, as seen in Table 1. This means that the fabrication method gives reproducible CPCs.

The CPCs were optically characterized to see how the deviation, i.e., increased length and diameter may have affected their optical performance. Fluorescence spectra from CPC batch 1 and a plane cut fiber tip is shown in Fig. 12. It is seen that the fluorescence intensity increases for CPCs, but that not all the CPCs performed in a similar manner.

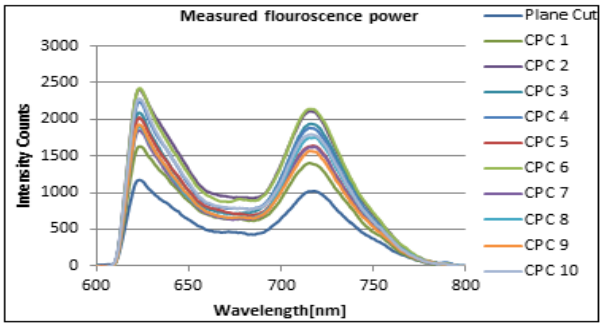

Fig. 12. Fluorescent spectrum for assay and reference fluorescence of batch 1 and plane cut fiber tip.

The spectrum for batch 1 is normalized relative to the plane cut fiber reference in Fig. 13, which shows the overall increase in fluorescence power.

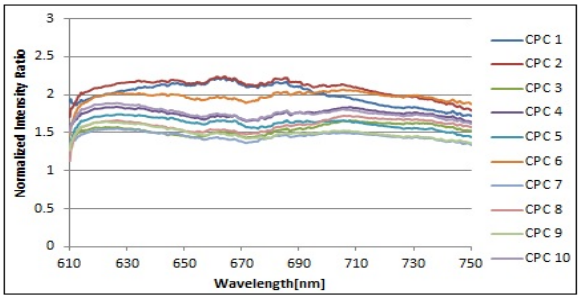

Fig. 13. Fluorescence spectrum normalized to plane cut fiber measured spectrum.

The average increase in the fluorescence intensity and the standard deviation of the increment factor in each batch is summarized in Table 2. In average, both CPC batches showed an improvement by a factor of ~1.7 in the received fluorescence, compared to a plane cut fiber tip. The relatively low standard deviation in the increment factor suggests that the CPCs are reproducible in performance.

Table 2. Increased in detected fluorescent power for two batches compared to plane cut fiber tip.

Increment factor	**Batch 1**	**Batch 2**
Batch Average	1.72	1.76
Standard Deviation	0.28	0.24
Confidence Interval (95%)	[1.57; 1.87]	[1.60; 1.92]

#250279 Received 17 Sep 2015; revised 16 Nov 2015; accepted 18 Nov 2015; published 20 Nov 2015

We know from previous simulations that if the CPC is within the required specifications, the increase should be close to 3 times for a fiber length of 35 mm. Some CPCs showed an increment factor of more than 2 while others show less than 1.5. On average the measured increment factor is less than the predicted value from simulations.

The predictions of the increment factor of the Zemax modelling that should be obtained using an ideal CPC shape are more than 40% above the measured values. To see if the discrepancy is solely due to the non-ideal shape and not fundamental to the modelling, we reconstructed the CPC 2 (best CPC of batch 1 showing an increment factor of 2.1 at 35mm) with the Zemax freeform optics feature using the real CPC coordinates. The CPC coordinates were measured from the CPC radius at different positions, as shown in Fig. 14(a).

We then used the real non-ideal CPC 2 shape in the Zemax model, in order to compare its increment factor of fluorescence with the ideal CPC shape. The results shown in Fig. 14(c) confirm that the simulation result for the real CPC 2 are different from the ideal results and in close agreement with the measured increment factor at 35 mm. This shows that the variation in the CPC geometrical parameters is the primary reason for the reduction in the CPC performance, and not the assumptions made in the modelling.

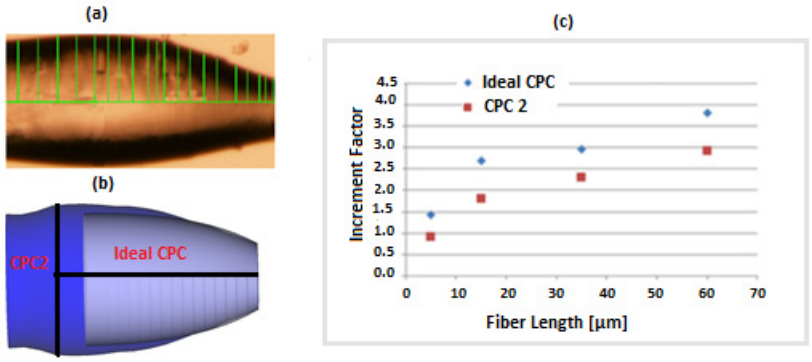

Fig. 14. (a) Image of CPC 2 with indication of the 26 radius measurement points. (b) Reconstructed and ideal CPC 2 shapes. (c) Increment factor comparison of ideal and real CPC 2 for different fiber lengths.

In Fig. 15 we investigate further the influence of the CPC length and maximum diameter on the increment factor. As already mentioned we see that CPC 2, which has the parameters closest to the ideal, has also the largest increment factor. Besides this fact, it is difficult to see any correlation from the plot. We therefore used statistics to find the correlation factors given in Table 3. A correlation coefficient of −1 indicates a perfect negative correlation, i.e., if a variable X increases, then the variable Y decreases and vice versa.

Table 3. Correlation among the CPC length, maximum diameter, and increment factor

	Correlation coefficient
Increment Factor & CPC Length	−0.74
Increment Factor & Maximum Diameter	−0.37
CPC Length & Maximum Diameter	−0.13

#250279 Received 17 Sep 2015; revised 16 Nov 2015; accepted 18 Nov 2015; published 20 Nov 2015

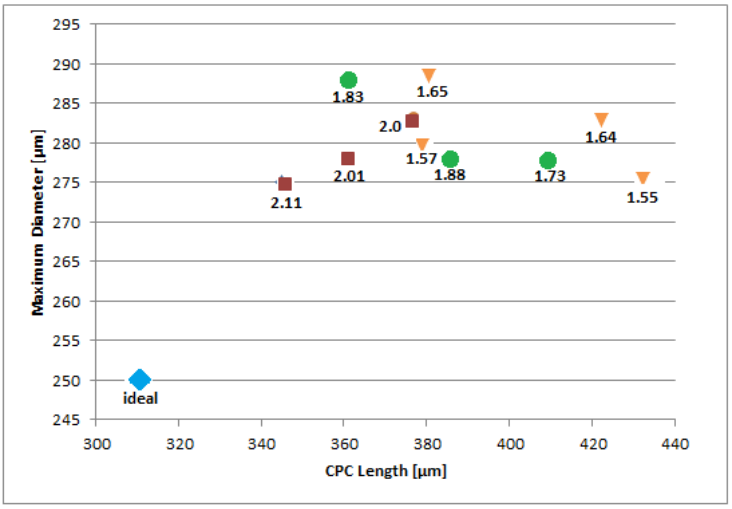

Fig. 15. Increment factor spread for CPC Length vs Maximum CPC diameter.

From the correlation factors we see that the most important parameter for a good increment factor is the CPC length, which has a correlation factor of −0.74. As anticipated the two geometrical parameters are not significantly correlated themselves, with only a correlation factor of −0.13.

Conclusion

A simple method has been proposed for the fabrication of polymer optical fiber CPC tips for a FRET based glucose sensor. The method makes the CPCs by tapering the fiber and without removing the fiber cladding. The produced CPC has been demonstrated to improve the fluorescence pickup efficiency and the received fluorescence power by an average factor of 1.74 for a non-optimal fiber length of 35mm chosen to physical requirements. The fabrication method gives reproducible CPC tips, which have, however, a larger maximum diameter and longer length than the ideal shape. Zemax modelling on the ideal shape predicts an improvement factor of 3 in the received power, whereas Zemax modelling on the real reconstructed best performing CPC shape confirms the measured increment factor of 2.11. With further optimization of the fabrication process it should therefore be possible to achieve the maximum predicted improvement of a factor of 3.

Acknowledgments

The research leading to these results has received funding from the People Programme (Marie Curie Actions) of the European Union's Seventh Framework Programme FP7/2007-2013/ under REA grant agreement n° 608382.

#250279 Received 17 Sep 2015; revised 16 Nov 2015; accepted 18 Nov 2015; published 20 Nov 2015